



Contents lists available at ScienceDirect

Biochemical and Biophysical Research Communications

journal homepage: [www.elsevier.com/locate/ybbrc](http://www.elsevier.com/locate/ybbrc)

# Identification of protein tyrosine phosphatase 1B (PTP1B) inhibitors through De Novo Evoluton, synthesis, biological evaluation and molecular dynamics simulation

Jingwei Wu<sup>1</sup>, Yangchun Ma<sup>1</sup>, Hui Zhou, Liang Zhou, Shan Du, Yingzhan Sun, Weiya Li, Weili Dong\*, Runling Wang\*\*

Tianjin Key Laboratory on Technologies Enabling Development of Clinical Therapeutics and Diagnostics (Theranostics), School of Pharmacy, Tianjin Medical University, Tianjin, 300070, China

## ARTICLE INFO

### Article history:

Received 1 March 2020

Accepted 12 March 2020

Available online xxx

### Keywords:

PTP1B

Type-2 diabetes mellitus

Computer aided drug design

De Novo Evoluton

Molecular dynamics simulation

## ABSTRACT

Protein tyrosine phosphatase 1B (PTP1B) is a widely expressed 50 kDa enzyme and the first intracellular PTP to be purified from human placental tissue. It has been proved that protein tyrosine phosphatase 1B played a significant role in the negative regulation of insulin signaling pathway and overexpression of PTP1B could lead to the decrease of insulin resistance. Therefore PTP1B has emerged as a novel promising therapeutic target for the treatment of type-2 diabetes mellitus. Computer aided drug design (CADD), chemical synthesis and biological activity assay resulted in the identification of a novel potent PTP1B inhibitor, compound **1a**, which shared an IC<sub>50</sub> value of 4.46 μM. Finally, the analysis of molecular dynamics simulation provided the theoretical basis for favorable activity of compound **1a**.

© 2020 Elsevier Inc. All rights reserved.

## 1. Introduction

Diabetes mellitus, the major threat to human health worldwide, is a chronic disease that results from either insulin deficiency or insulin resistance, or both [1]. The World Health Organization (WHO) reports indicated that there were 425 million new cases of diabetes around the world in 2017 and the global prevalence was projected to continue to rise to 629 million by 2045 [2]. However, cases of diabetes are on the rise, and its complications are torturing and killing more and more people. type-2 diabetes mellitus is noninsulin-dependent diabetes mellitus and characterized by insulin resistance (IR) and relatively lack of insulin [3].

Protein tyrosine phosphatases (PTPs) are a group of enzymes regulating the dephosphorylation of tyrosine (Tyr)-phosphorylated proteins and the cellular function [4]. A lot of PTPs can function either as positive or negative modulators in a variety of signal transduction pathways [5]. Protein tyrosine phosphatase 1B (PTP1B), the first purified PTP, is a widely expressed 50 kDa enzyme

and localized mainly in the endoplasmic reticulum [6]. It has been proved that protein tyrosine phosphatase 1B played a significant role in the negative regulation of insulin signaling pathway and overexpression of PTP1B could lead to the decrease of insulin resistance [7]. Another evidence for the correlation between insulin resistance and PTP1B was provided by PTP1B knockout mice, which could improve glucose tolerance and insulin sensitivity [8]. Hence, PTP1B has emerged as a novel promising therapeutic target for the treatment of T2-DM.

Recently, a lot of novel PTP1B inhibitors have been developed by research institutions, including carboxylic acids, phosphonic acids, sulphonic acids, imides, phosphonodifluoromethyl phenylalanine derivatives and vanadium compounds [9]. Among them, several drug candidates have been developed by pharmaceutical companies, such as TTP-814, ISIS 113715, MSI-1436, way-123783, ISIS-PTP1BRx and MSI-1436 [9,10]. However, the reported inhibitors cause some side effects and do not have sufficient potency to demonstrate *in vivo* activity [11,12]. Hence, it is still a challenge to discover potent, permeable, selective PTP1B inhibitors for treating type-2 diabetes mellitus.

In view of this situation, we designed a series of PTP1B inhibitors with the aid of virtual screening, De Novo Evolution, docking and ADMET (absorption, distribution, metabolism, excretion and toxicity) validating. For purpose of finding novel potent PTP1B

\* Corresponding author.

\*\* Corresponding author.

E-mail addresses: [dongweili@tmu.edu.cn](mailto:dongweili@tmu.edu.cn) (W. Dong), [wangrunling@tmu.edu.cn](mailto:wangrunling@tmu.edu.cn) (R. Wang).<sup>1</sup> These authors contributed equally to this work.

inhibitors for the treatment of T2-DM, a classes of ethyl 4-(substitutedphenoxy)methylthiazole-5-carboxylates were synthesized. Then, the PTP1B biological activity was tested. Meanwhile, molecular dynamics simulations and several post-analysis experiments were carried out to analyze the binding interactions between PTP1B and the desired compounds, such as the root mean square deviation analysis (RMSD), the root mean square fluctuation analysis (RMSF), principal component analysis (PCA) and Domain cross-correlation map (DCCM) analysis. The flow chart of the test procedure was shown in Fig. 1. Hopefully, the findings could provide useful insights for developing novel potent PTP1B inhibitors against type-2 diabetes mellitus and provide promising potential drug candidate.

## 2. Materials and methods

### 2.1. Virtual screening

Docking-based virtual screening has been proved to be an effective tool in the process of drug design and optimization and widely used in the development of new drugs [13]. For the sake of high-level efficiency [14], the protocol of “LibDock” was selected to perform virtual screening in this paper. The PTP1B protein structure (2QBQ) [15] downloaded from the RCSB PDB library needs to prepare with the protocol of “Prepare Protein”. Meanwhile, the protocol of “Prepare Ligands” was used to prepare the small molecules retrieved from ZINC database. Finally, the prepared ligands were docked into the active site sphere, which contains P-loop (residues Thr177-Ser187) and WPD-loop (residues His214-Arg221) [16]. According to the docking score, the best hit was used to generate derivatives with the method of “De Novo Evolution”.

### 2.2. De Novo Evolution

In order to design potent PTP1B inhibitors containing novel scaffolds, the protocol of “De Novo Evolution” based on Ludi algorithm was carried out by evaluating fragments that best complement the receptor [17]. The fragments which complement to the receptor were added to the existing scaffold and the binding affinity to PTP1B would be improved [18,19]. The procedure of “De Novo Evolution” could be divided into four steps. Firstly, the conformation of the PTP1B and the scaffold is calculated by the CHARMM position [20]. Secondly, the “De Novo Library Generation” module was selected to generate fragment libraries. Thirdly, “De novo receptor” protocol was applied to find the binding site of

PTP1B. Fourthly, the procedure of “De Novo Link” was adopted to add appropriate fragments to the existing scaffold. The maximum generation of designed derivatives was set to 1000. Finally, the generated derivatives in the top 100 scored were then forward for the protocol of “CDOCKER”.

### 2.3. Molecular docking

Molecular docking technology is an important part of structure-based drug design, which can find the best binding mode between receptor and ligand according to the principle of geometric complementarity, energy complementarity, and chemical environment complementarity. Many docking methods have been reported in recent years and some useful comparisons of the re-docking ability of these algorithms have been published [21]. CDOCKER exhibited the best performing among the reported docking software for the high accuracy of docking and scoring [22]. Since that is so, the generated derivatives in the top 100 scored were re-docked into to the PTP1B binding pocket by the protocol of “CDOCKER”. According to the -CDOCKER\_ ENERGY, the best hits were adopted to perform the procedure of ADMET prediction.

### 2.4. Absorption, distribution, metabolism, excretion and toxicity (ADMET) prediction

Here we investigated the ADMET features by performing “ADMET Descriptions” protocol to estimate the following properties: the logarithm of the partition coefficient between n-octanol and water (CLogP), aqueous solubility blood-brain barrier (BBB) penetration, absorption level, plasma protein binding (PPB) and CYP450 2D6 inhibition [23]. The potential candidates were then forward for chemical synthesis and biological activity assay.

### 2.5. Chemistry

The synthetic route to the desired products **1a-1j** is illustrated in Schemes 1. The detailed information for the synthesis of intermediate (**3a-3e** and **4a-4e**) was listed in the supporting information.

Reagents and conditions: (i).ethyl 2-chloro-3-oxobutanoate, EtOH, reflux; (ii). NBS, AIBN, CCl<sub>4</sub>, 80 °C; (iii). 4-substitute phenol, K<sub>2</sub>CO<sub>3</sub>, MeCN, reflux.

Synthesis of target compounds **1a-1j**: A mixture of **4a-4e** (3 mmol), 4-substitute phenol (3.6 mmol) and K<sub>2</sub>CO<sub>3</sub> (6 mmol, 0.83 g) in MeCN (10 mL) was stirred at reflux until the completion of reaction as indicated by TLC analysis [24].

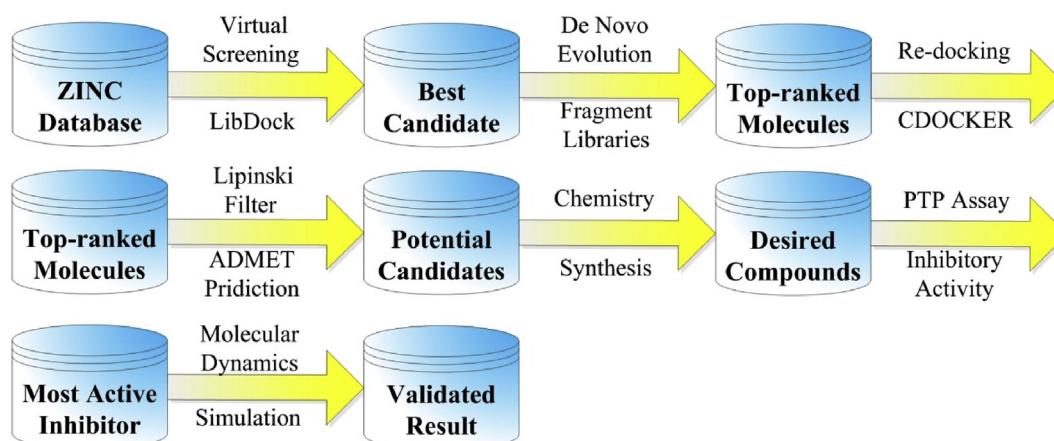
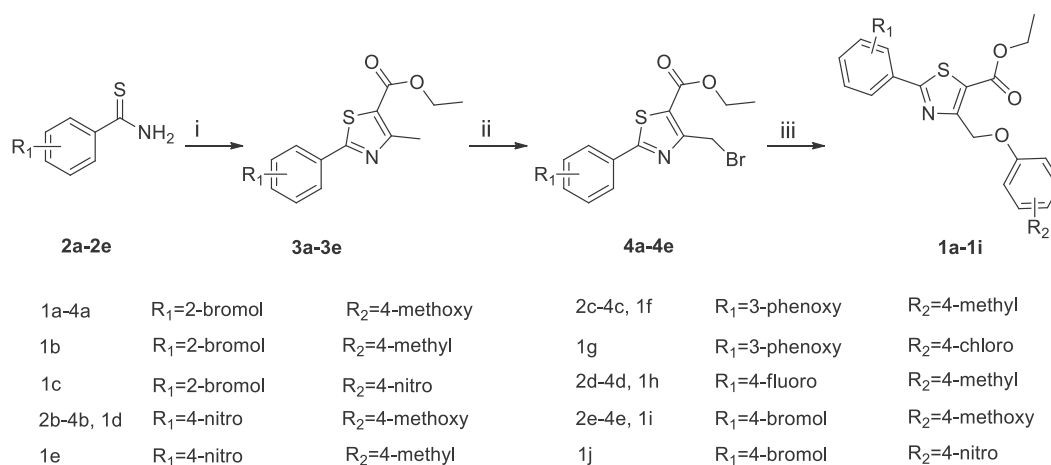


Fig. 1. The flowchart of the test procedure.

Scheme 1. Synthetic routes to target compounds **1a-1j**.

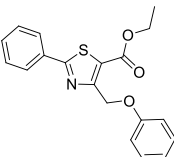
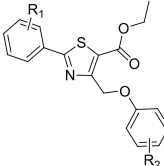
After cooling to room temperature, the volatiles were removed under reduced pressure, and the resulting residue was diluted with CH<sub>2</sub>Cl<sub>2</sub> (30 mL), H<sub>2</sub>O (30 mL). The phases were separated and the aqueous was further extracted with CH<sub>2</sub>Cl<sub>2</sub> (30 mL × 3). The combined extracts were dried over anhydrous Na<sub>2</sub>SO<sub>4</sub> and concentrated. Finally, the resulting residue was purified by silica chromatography by EtOAc/*n*-hexane (1/5 by v/v) to afford **1a-1j**. The NMR/MS spectra datas were listed in the [supporting information](#).

## 2.6. Biological evaluation

The inhibitory activity of PTP1B, TCPTP, PTP-LAR, CDC25B, SHP1 and MEG2 were tested in 96-well plates at 37 °C and p-nitrophenyl phosphate (pNPP) activity was measured according to the release of p-nitrophenyl from p-nitrophenylphosphate, which was determined spectrophotometrically at 405 nm [25]. The reaction mixture contained 1 mM-(Ethylenedinitrilo)tetraacetic acid, 10 mM-

Table 1

Molecular docking results for the derivatives (top-10) generated by de novo evolution protocol from ZINC39276654 (scaffold).

	De Novo Evolution				
ZINC39276654	compound 1a-1j				
Name	R <sub>1</sub>	R <sub>2</sub>	MW	Ludi SCORE	-CDOCKER ENERGY
<b>ZINC39276654</b>	-	-	339.41	-	31.78
<b>1a</b>	2-bromol	4-methoxy	448.33	820	59.94
<b>1b</b>	2-bromol	4-methyl	432.33	875	53.30
<b>1c</b>	2-bromol	4-nitro	463.30	943	49.77
<b>1d</b>	4-nitro	4-methoxy	414.43	781	55.31
<b>1e</b>	4-nitro	4-methyl	398.43	808	53.15
<b>1f</b>	3-phenoxy	4-methyl	445.53	944	50.26
<b>1g</b>	3-phenoxy	4-chloro	465.95	912	57.34
<b>1h</b>	4-fluoro	4-methyl	371.43	795	49.05
<b>1i</b>	4-bromol	4-methoxy	448.44	825	56.28
<b>1j</b>	4-bromol	4-nitro	463.30	819	51.11

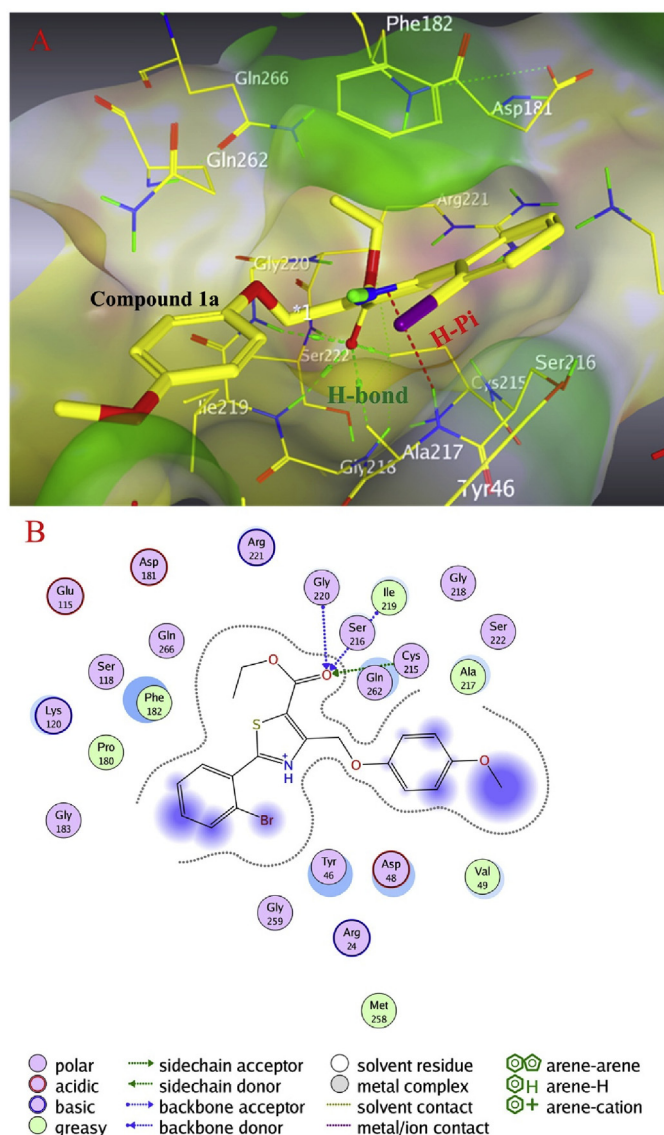


**Fig. 2.** Structures and binding interactions of PTP1B in complex with compound **1a**. (A) Surface representation of PTP1B in complex with compound **1a** (green). Hydrogen bond interactions were depicted as green-dashed lines; H-Pi interaction was depicted as red-dashed lines. (B) 2D diagram of the interaction of compound **1a**-PTP1B. (For interpretation of the references to color in this figure legend, the reader is referred to the Web version of this article.)

**Table 2**  
The ADMET prediction for the target compounds.

Name	CLogP	Solubility level <sup>a</sup>	CYP2D6 Prediction	BBB-Level <sup>b</sup>	Hepatotoxicity# Prediction	PPB Prediction	Absorption -level <sup>d</sup>
1a	5.545	3	False	0	False	True	good
1b	5.955	3	False	1	False	True	good
1c	5.499	3	False	1	False	True	moderate
1d	4.728	4	False	0	False	True	moderate
1e	5.138	3	False	1	False	True	good
1f	7.488	2	False	2	False	True	moderate
1g	7.842	2	False	0	False	True	good
1h	5.535	3	False	2	False	True	poor
1i	5.845	3	False	1	False	True	good
1j	5.799	3	False	1	False	True	moderate

<sup>a</sup> Solubility level: 0-extremely low; 1-very low, but possible; 2-low; 3-good; 4-optimal.

<sup>b</sup> BBB level: 0-very good; 1-good; 2-moderate; 3-poor; 4-undefined.

pNPP, 50 mM-citrate, 0.1M-sodium chloride, and 1 mM-DL-dithiothreitol and incubated for 40 min at 37 °C. The reaction was stopped by the addition of 5  $\mu$ L of 1M-NaOH.

## 2.7. Molecular dynamics simulations

The methods of molecular dynamics simulations have been listed in the [supporting information](#).

## 3. Results and discussion

### 3.1. Compounds design

It could be seen from [Fig. 1](#) and [Table 1](#) that ZINC39276654 was identified in the protocol of LibDock-based virtual screening. As the best scaffold, ZINC39276654 produced 1000 molecules by the “De Novo Evolution” procedure. Then the generated derivatives in the top 100 scored were selected and re-docked into the receptor (PTP1B) to compute the -CDOCKER\_ENERGY by the protocol of “CDOCKER” According to the -CDOCKER\_ENERGY, the results of top 10 compounds (**1a-1j**) and ZINC39276654 (scaffold) were shown in [Table 1](#). The -CDOCKER\_ENERGY includes ligand-receptor interaction energy and internal ligand strain energy. The higher the value, the more favorable the binding mode [26]. It is obvious that the compounds **1a-1j** shared the more favorable binding mode than ZINC39276654 (scaffold). Among them, compound **1a** shared the highest -CDOCKER\_ENERGY (59.94) and was used to the following analysis of docking conformation and binding interactions.

As shown in [Fig. 2A](#), the oxygen atoms of compound **1a** formed four H-bonds with the residues of Cys215, Ser216, Ile219 and Gly220 (green-dashed arrow in [Fig. 2A](#)), which were all in the active site of PTP1B. The compound **1a** could also generate H-Pi interactions (red-dashed arrow in [Fig. 2A](#)) with the residue of Ala217. As shown in [Fig. 2B](#), it was obviously that the compound **1a** could embed well into the active pocket of PTP1B and left a fraction of the atoms in the state of exposure (blue shadows of the ligand), resulting in the strong binding affinities. Greasy residues were shown as green circles (Val49, Pro180, Phe182, Ala217, Ile219 and Met258) while polar residues were shown as pink circles (Tyr46, Ser118, Gly183, Cys215, Ser216, Gly218, Gly220, Arg221, Ser222, Gly259, Gln262 and Gln266).

### 3.2. ADMET prediction

We also investigated the ADMET prediction by performing “ADMET Descriptions” protocol to estimate the following



**Table 3**Inhibitory activity of compound **1a-1j** and ZINC39276654 against PTP1B and other phosphatases.

Compounds	PTP1B IC <sub>50</sub> (μM)	TCPTP IC <sub>50</sub> (μM)	SHP1 IC <sub>50</sub> (μM)	MEG2 IC <sub>50</sub> (μM)	CDC25B IC <sub>50</sub> (μM)	LAR IC <sub>50</sub> (μM)
ZINC39276654	>100	>100	>100	>100	>100	>100
<b>1a</b>	4.46	12.28	>100	>100	>100	>100
<b>1b</b>	10.41	31.02	>100	>100	>100	>100
<b>1c</b>	10.79	>100	>100	>100	>100	>100
<b>1d</b>	11.58	38.65	>100	>100	>100	>100
<b>1e</b>	12.05	36.68	>100	>100	>100	>100
<b>1f</b>	11.22	35.91	33.26	>100	>100	>100
<b>1g</b>	10.73	>100	>100	>100	>100	>100
<b>1h</b>	9.69	39.35	39.08	>100	>100	>100
<b>1i</b>	8.03	27.68	>100	>100	>100	>100
<b>1j</b>	64.75	>100	>100	>100	>100	>100

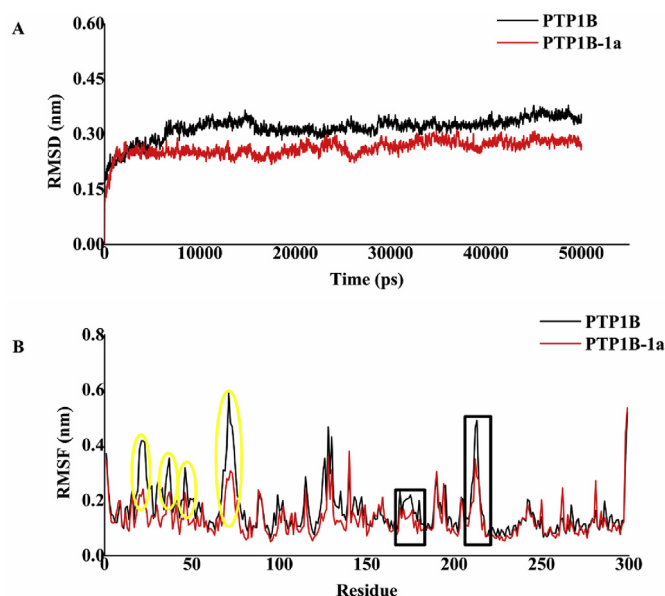


**Fig. 3.** (A) Standard RMSD of PTP1B system and PTP1B-1a system. (B) RMSF during 3–50 ns. The PTP1B system is in black solid line and the PTP1B-1a complex system is in red solid line. Large difference between areas marked by yellow and black boxes. (For interpretation of the references to color in this figure legend, the reader is referred to the Web version of this article.)

properties: the logarithm of the partition coefficient between n-octanol and water (ClogP), aqueous solubility blood-brain barrier (BBB) penetration, absorption level, plasma protein binding (PPB) and CYP450 2D6 inhibition. It could be seen from Table 2 that most compounds exhibited moderate or good human intestinal absorption except **1h** (poor level). The distribution properties were calculated using predictive plasma protein binding, which was widely used because the degree of plasma protein binding of a drug has an important role on its disposition and the drug's efficacy [27]. Fortunately, the compounds **1a-1j** exhibited good PPB properties. For hepatotoxicity, ten compounds (**1a-1j**) were predicted non-toxic. It was obviously that compounds **1a-1j** exhibited acceptable pharmaceutical properties, so the potential candidates were then forward for chemical synthesis and biological activity assay.

### 3.3. Biological evaluation

The results of biological evaluation of compounds **1a-1j** and ZINC39276654 (scaffold) on PTP1B were listed in Table 3. It was obviously that the inhibitors **1a-1i** showed better PTP1B inhibitory activity (IC<sub>50</sub> values were range from 4.46 μM to 12.05 μM) than ZINC39276654 (IC<sub>50</sub> > 100 μM) while compound **1j** showed similar

inhibitory activity (IC<sub>50</sub> = 64.75 μM) to ZINC39276654. Besides, it was clear that the worst and the best R<sub>2</sub> group were 4-nitro and 4-methoxy (**1a** > **1b** > **1c**, **1d** > **1e**, **1i** > **1j**), while the best and the worst R<sub>1</sub> group were 2-bromol and 4-bromol respectively (**1a** > **1i**, **1c** > **1j**). Besides, the biological evaluation of inhibitors **1a-1j** led to the development of a novel structure PTP1B inhibitor **1a**, which shared an IC<sub>50</sub> value of 4.46 μM.

In order to investigate the selectivity of the compounds **1a-1j**, their biological activity on similar PTPs were assayed, which consisted of TCPTP, SHP1, CDC25B, LAR and MEG2. It was very clear that compounds **1a-1i** did not show any promising activity on CDC25B, MEG2 and LAR. Meanwhile compounds **1f** and **1h** exhibited moderate SHP1 inhibitory activity (IC<sub>50</sub> = 33.26 μM for **1f**, IC<sub>50</sub> = 39.08 μM for **1h**). Compound **1c** and **1g** exhibited favorable selectivity (more than 10-fold) for PTP1B over TCPTP, seven compounds (**1a-1b**, **1d-1f**, **1h-1i**) showed moderate selectivity (2.8-fold–4.1-fold). Unfortunately, compound **1j** did not show any selectivity. Among the desired compounds, compound **1g** showed the strongest selectivity for PTP1B over the other phosphatases.

### 3.4. Molecular dynamics simulations

#### 3.4.1. Root mean square deviation (RMSD)

In this study, the trace files of the MD simulation were used to perform RMSD analysis on the PTP1B protein system and the protein ligand complex system, respectively. The results of RMSD analysis can be used as a measure to evaluate the overall fluctuation of the protein's main chain atoms. The value of RMSD has a negative correlation with the stability of the main chain atoms. The larger the value of RMSD, the more unstable the main chain atoms are. It can be found in Fig. 3A that the protein system tends to stabilize after 3 ns, so the MD file after 3 ns is used for MD simulation analysis. In the SHP2 system, the average RMSD of 3–50 ns is 0.317 nm. However, in the protein-ligand complex (PTP1B-1a) system, the mean value of RMSD of 3–50 ns is 0.281 nm. In comparison, the average RMSD of the PTP1B-1a complex system is lower. At the same time, it can be clearly found that the overall fluctuation of RMSD of the protein-ligand complex system is lower than that of the PTP1B system in Fig. 3A, which indicates that the protein-ligand complex system is more stable. Therefore, the simultaneous effects of compound **1a** and active sites have stabilized the overall conformation of the PTP1B protein.

#### 3.4.2. Root mean square fluctuation (RMSF) analyses

In order to better study the effect of compound **1a** on the active regions of the side chain atoms of the PTP1B protein, RMSF analysis technology was applied to analyze the trajectory files generated by MD simulations. Fig. 3B is a graph of RMSF data generated by the PTP1B system and the protein-ligand complex system in 3–50 ns. The RMSF value also has a negative correlation with the side chain

atoms. The smaller the RMSF value, the more stable the side chain atoms. The areas with large differences in RMSF fluctuations in the two systems were marked with a yellow box and a black box, respectively. The amino acid regions marked by yellow boxes were residue Ser50-Arg56, Thr154-Thr164. However, since the region marked by the yellow ellipse was not in the active site region, it will not be discussed in detail. The areas marked by the black square boxes were residue Val113-Ser118 (R-loop), Thr177-Pro185 (WPD-loop) and His214-Arg221 (active site). It can be seen from Fig. 3B that the RMSF fluctuations in the black box regions have significant differences (RMSF value of the protein-ligand complex system less

than PTP1B system). The average RMSF values of residues Val113-Ser118, Thr177-Pro185, and His214-Arg221 in the PTP1B protein were 0.180 nm, 0.132 nm, and 0.138 nm, respectively, while in the PTP1B-1a system, 0.125 nm, 0.102 nm, and 0.120 nm, respectively. Obviously, the fluctuation of RMSF in the PTP1B-1a system was significantly lower than that in the PTP1B system, which indicates that the side chain residues in the protein-ligand complex system become more stable. It is worth noting that the residues Val113-Ser118, Thr177-Pro185, and His214-Arg221 are all around the active pocket, which suggests that compound 1a makes the active site of the PTP1B protein more stable.

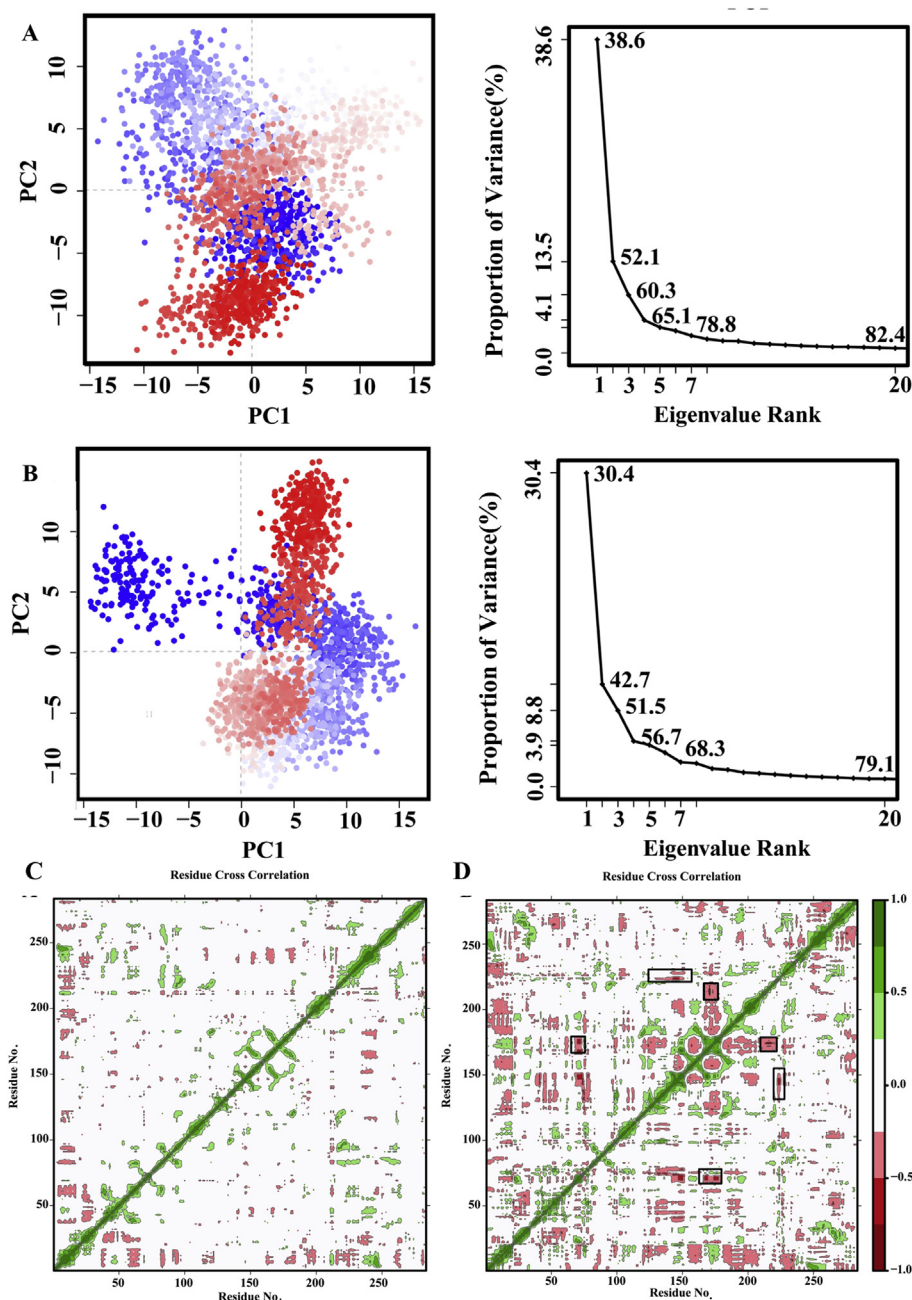


**Fig. 4.** Principal component analysis. Projection of trajectories into PC1 and PC2 for (A) PTP1B system (B) PTP1B-1a complex system. (C) DCCM for the PTP1B-1a system showing positive and negative correlative motions between the residues. (D) DCCM for PTP1B-1a complex system showing positive and negative correlative motions between residues. Green represents positive correlations, whereas red represents negative correlations. (For interpretation of the references to color in this figure legend, the reader is referred to the Web version of this article.)

### 3.4.3. Conformation transitions of the PTP1B protein and PTP1B-1a system

PCA analysis makes the three-dimensional conformational information of PTP1B more intuitive in the two-dimensional plane, which is more conducive to the analysis of the conformational state of PTP1B in the 3–50 ns MD simulation. The anharmonic and large-scale motions in proteins are closely related to biological functions, so the anharmonic and large-scale motions of proteins are separated from other motions by diagonalization of covariance matrix and reflected in the form of eigenvalue eigenvectors. It can be found in Fig. 4 that in the MD simulation of 3–50 ns, the top 20 ps of PTP1B system and PTP1B-1a system account for 82.4% and 79.1% of the total variation respectively. In the PTP1B system, the first two PC (PC1, PC2) eigenvectors account for 38.6% and 13.5% of the total variation respectively, while the other PCs account for no more than 8.2% of the maximum. In the PTP1B-1a system, PC1 and PC2 account for 30.4% and 12.3% respectively, while other PCs account for no more than 8.8%. Obviously, PC1 and PC2 account for most of the protein fluctuations. Therefore, PCA dots images generated from the first two eigenvectors are used to observe the conformational changes of PTP1B. The blue and red dots in Fig. 4 represent different conformational states of PTP1B protein, while the white dots represent the unstable intermediate state of PTP1B protein. It can be found from Fig. 4A that the points of PTP1B system are evenly distributed near the midline, while the points of PTP1B-1a system (Fig. 4B) are concentrated on both sides of the midline. The closer the point distribution in Fig. 4 indicates that the protein system is more stable, so the PTP1B-1a system is in a more stable state. In conclusion, the binding of compound 1a has a stable effect on the conformation of PTP1B. PCA scores are consistent with the above analysis results.

### 3.4.4. The correlation motion of the PTP1B protein and PTP1B-1a system

From the above analysis results, it can be inferred that the fluctuation of WPD loop and active site in PTP1B-1a system is significantly reduced. In order to further explore the fluctuation of these two regions in PTP1B, DCCM data generated from 3 to 50 ns MD simulation was used to analyze the movement trend of C $\alpha$  atom in the dynamic simulation process. In Fig. 4C, the abscissa and ordinate are arranged according to the sequence of amino acid residues, and the relationship between the upper left corner and the upper right corner is symmetrically distributed according to the diagonal. The correlation motion and anti-correlation motion between specific residues are represented by green (syn motion) and red (anti motion) respectively, and the intensity of correlation motion is positively correlated with the depth of color. In Fig. 4D, the regions with significant differences in correlation between WPD loop and active sites were labeled with black boxes. Obviously, in PTP1B-1a complex system (Fig. 4D), the interaction between amino acid residues was enhanced obviously, indicating that compound 1a enhanced the correlation within the protein. In PTP1B-1a complex system, the WPD loop (Thr177-Pro185) of the protein formed a strong anti-correlation, which was different from the residues Ser70-Glu75 and active site (His214-Arg211), but the anti-correlation was weakened or disappeared in PTP1B protein system. In the PTP1B-1a complex system, active site (His214-Arg211) and residue Glu200-Ser205 form a strong anti-correlation, while in the PTP1B protein system, the anti-correlation is weakened. The enhancement of the anti-correlation of the above regions indicated that the amino acid residues moved in the opposite direction. In a word, we can find that the anti-correlation between WPD loop and active site area is significantly enhanced, which indicates that the interaction between amino acid residues in these two areas is increased, which will make the protein in a more stable state.

## 4. Conclusions

Computer aided drug design (CADD), chemical synthesis and biological activity assay resulted in the identification of a novel potent PTP1B inhibitor, compound 1a which shared which shared an IC<sub>50</sub> value of 4.46  $\mu$ M. Among the desired compounds 1a–1j, compound 1g showed the strongest selectivity for PTP1B over the other phosphatases while compound 1j did not show any selectivity. Finally, the analysis of molecular dynamics provided the theoretical basis for favorable activity of compound 1a.

## Declaration of competing interest

There is no conflict of interest.

## Acknowledgments

This study was supported by the National Natural Science Foundation of China (Grant No. 81773569), the Natural Science Foundation of Tianjin City, China (Grant No. 18JCQNJC13700).

## Appendix A. Supplementary data

Supplementary data to this article can be found online at <https://doi.org/10.1016/j.bbrc.2020.03.075>.

## References

- [1] H.C. Kenny, E.D. Abel, Heart failure in type 2 diabetes mellitus: impact of glucose-lowering agents, heart failure therapies, and novel therapeutic strategies, *Circ. Res.* 124 (2019) 121–141, <https://doi.org/10.1161/CIRCRESAHA.118.311371>.
- [2] N.G. Forouhi, N.J. Wareham, Epidemiology of diabetes, *Medicine* 47 (2019) 22–27, <https://doi.org/10.1016/j.mpmed.2018.10.004>.
- [3] J. Sun, C. Qu, Y. Wang, et al., PTP1B, a potential target of type 2 diabetes mellitus, *Mol. Biol.* 5 (2016) 174, <https://doi.org/10.4172/2168-9547.1000174>.
- [4] N.K. Tonks, Protein tyrosine phosphatases: from genes, to function, to disease, *Nat. Rev. Mol. Cell Biol.* 7 (2006) 833–846, <https://doi.org/10.1038/nrm2039>.
- [5] L.R. Bollu, A. Mazumdar, M.I. Savage, et al., Molecular pathways: targeting protein tyrosine phosphatases in cancer, *Clin. Canc. Res.* 23 (2017) 2136–2142, <https://doi.org/10.1158/1078-0432.CCR-16-0934>.
- [6] H. Cho, Protein Tyrosine Phosphatase 1B (PTP1B) and Obesity, *Vitamins & Hormones*, Elsevier, 2013, pp. 405–424, <https://doi.org/10.1016/B978-0-12-407766-9.00017-1>.
- [7] G.K. Kuga, V.R. Muñoz, R.C. Gaspar, et al., Impaired insulin signaling and spatial learning in middle-aged rats: the role of PTP1B, *Exp. Gerontol.* 104 (2018) 66–71, <https://doi.org/10.1016/j.exger.2018.02.005>.
- [8] B. Boivin, R.S. Sagabala, Role of cholesterol and oxysterols in regulating PTP1B activity, *Free Radic. Biol. Med.* 112 (2017) 146, <https://doi.org/10.1016/j.freeradbiomed.2017.10.223>.
- [9] H. Hussain, L.R. Green, G. Abbas, et al., Protein tyrosine phosphatase 1B (PTP1B) inhibitors as potential anti-diabetes agents: patent review (2015–2018), *Expert Opin. Ther. Pat.* 29 (2019) 689–702, <https://doi.org/10.1080/13543776.2019.1655>.
- [10] L.-J. Wang, B. Jiang, N. Wu, et al., Small molecules as potent protein tyrosine phosphatase 1B (PTP1B) inhibitors documented in patents from 2009 to 2013, *Mini Rev. Med. Chem.* 15 (2015) 104–122, <https://doi.org/10.2174/1389557515666150203144339>.
- [11] Y. Han, M. Belley, C.I. Bayly, et al., Discovery of [(3-bromo-7-cyano-2-naphthyl)(difluoro) methyl] phosphonic acid, a potent and orally active small molecule PTP1B inhibitor, *Bioorg. Med. Chem. Lett.* 18 (2008) 3200–3205, <https://doi.org/10.1016/j.bmc.2008.04.064>.
- [12] L.R. Fiedler, Inhibiting the inhibitors, PTP1B as a therapeutic target in myocardial infarction, *Heart Res-Open J.* 5 (2018), <https://doi.org/10.17140/HROJ-5-147>.
- [13] J. Wu, Y. Sun, H. Zhou, et al., Design, synthesis, biological evaluation and molecular dynamics simulation studies of (R)-5-methylthiazolidin-4-One derivatives as megakaryocyte protein tyrosine phosphatase 2 (PTP-MEG2) inhibitors for the treatment of type 2 diabetes, *J. Biomol. Struct. Dynam.* (2019) 1–10, <https://doi.org/10.1080/07391102.2019.1654410>.
- [14] J. Wu, W. Li, Z. Zheng, et al., Design, synthesis, biological evaluation, Common feature pharmacophore model and molecular dynamics simulation studies of ethyl 4-(phenoxyethyl)-2-phenylthiazole-5-carboxylate as Src Homology-2 Domain Containing Protein Tyrosine Phosphatase-2 (SHP2) inhibitors, *J. Biomol. Struct. Dynam.* (2020) 1–29, <https://doi.org/10.1080/07391102.2020.1726817>.

- [15] D.P. Wilson, Z.-K. Wan, W.-X. Xu, et al., Structure-based optimization of protein tyrosine phosphatase 1B inhibitors: from the active site to the second phosphotyrosine binding site, *J. Med. Chem.* 50 (2007) 4681–4698, <https://doi.org/10.1021/jm0702478>.
- [16] S. Liu, L.-F. Zeng, L. Wu, et al., Targeting inactive enzyme conformation: aryl diketoacid derivatives as a new class of PTP1B inhibitors, *J. Am. Chem. Soc.* 130 (2008) 17075–17084, <https://doi.org/10.1021/ja8068177>.
- [17] T.-T. Chang, M.-F. Sun, H.-Y. Chen, et al., Screening from the world's largest TCM database against H1N1 virus, *J. Biomol. Struct. Dynam.* 28 (2011) 773–786, <https://doi.org/10.1080/07391102.2011.10508605>.
- [18] Y. Jiang, H. Gao, Pharmacophore-based drug design for the identification of novel butyrylcholinesterase inhibitors against Alzheimer's disease, *Phyto-medicine* 54 (2019) 278–290, <https://doi.org/10.1016/j.phymed.2018.09.199>.
- [19] C.Y.-C. Chen, Weighted equation and rules—a novel concept for evaluating protein-ligand interaction, *J. Biomol. Struct. Dynam.* 27 (2009) 271–282, <https://doi.org/10.1080/07391102.2009.10507315>.
- [20] B.R. Brooks, C.L. Brooks III, A.D. Mackerell Jr., et al., CHARMM: the biomolecular simulation program, *J. Comput. Chem.* 30 (2009) 1545–1614, <https://doi.org/10.1002/jcc.21287>.
- [21] J.B. Cross, D.C. Thompson, B.K. Rai, et al., Comparison of several molecular docking programs: pose prediction and virtual screening accuracy, *J. Chem. Inf. Model.* 49 (2009) 1455–1474, <https://doi.org/10.1021/ci900056c>.
- [22] J.K. Gagnon, S.M. Law, C.L. Brooks III, Flexible CDOCKER: development and application of a pseudo-explicit structure-based docking method within CHARMM, *J. Comput. Chem.* 37 (2016) 753–762, <https://doi.org/10.1002/jcc.24259>.
- [23] F. Cheng, W. Li, G. Liu, et al., In silico ADMET prediction: recent advances, current challenges and future trends, *Curr. Top. Med. Chem.* 13 (2013) 1273–1289, <https://doi.org/10.2174/15680266113139990033>.
- [24] J.-w. Wu, L. Yin, Y.-q. Liu, et al., Synthesis, biological evaluation and 3D-QSAR studies of 1, 2, 4-triazole-5-substituted carboxylic acid bioisosteres as uric acid transporter 1 (URAT1) inhibitors for the treatment of hyperuricemia associated with gout, *Bioorg. Med. Chem. Lett.* 29 (2019) 383–388, <https://doi.org/10.1016/j.bmcl.2018.12.036>.
- [25] J. Montalibet, K.I. Skorey, B.P. Kennedy, Protein tyrosine phosphatase: enzymatic assays, *Methods* 35 (2005) 2–8, <https://doi.org/10.1016/j.ymeth.2004.07.002>.
- [26] G. Wu, D.H. Robertson, C.L. Brooks III, et al., Detailed analysis of grid-based molecular docking: a case study of CDOCKER—a CHARMM-based MD docking algorithm, *J. Comput. Chem.* 24 (2003) 1549–1562, <https://doi.org/10.1002/jcc.10306>.
- [27] J. Dong, N.-N. Wang, Z.-J. Yao, et al., ADMETlab: a platform for systematic ADMET evaluation based on a comprehensively collected ADMET database, *J. Cheminf.* 10 (2018) 29, <https://doi.org/10.1186/s13321-018-0283-x>.